Evaluation of Corneal Shape and Biomechanics Before LASIK

Renato Ambrósio, Jr, MD, PhD
Leonardo P. Nogueira, MD
Diogo L. Caldas, MD
Bruno M. Fontes, MD
Allan Luz, MD
Jorge O. Cazal, MD
Milton Ruiz Alves, MD, PhD
Michael W. Belin, MD, FACS

Introduction

The preoperative evaluation is of critical importance for success in laser in situ keratomileusis (LASIK). This examination should fulfill 3 main purposes: counseling and educating the candidates, surgery planning, and screening for cases at higher risk for complications. It is critical to interview each refractive patient to assess their individual needs and to provide realistic expectations. A thorough ophthalmologic examination is mandatory, including specific complementary examinations to characterize many aspects of the cornea and the optics of the eye. In fact, it is notable that refractive surgery has motivated tremendous development for advanced diagnostic methods, among many others advancements and innovations in Ophthalmology.[1,2]

One of the most important aspects of the preoperative examination of LASIK candidates is to screen cases at risk for progressive ectasia.

INTERNATIONAL OPHTHALMOLOGY CLINICS
Volume 51, Number 2, 11–39

Keratectasia has emerged as a rare but very severe complication of LASIK, which is a leading cause of litigation.[3,4] In post-LASIK ectasia, the lamellar cut and excimer laser ablation lead to a state of biomechanical failure with an inability to support the continuous stresses caused by intraocular pressure (IOP), extraocular muscle action, blinking, eye rubbing, and other forces.[5] The corneal stroma undergoes a 2-step process of delamination and interfibril fracture, which is clinically characterized by thinning and bulging of the cornea. This causes mild-to-severe irregular astigmatism, a myopic shift, and typically reduces uncorrected and best spectacle-corrected visual acuity.[4] Considering the severity of such complication, prevention is the best approach.

Refractive surgeons routinely face the challenges of identifying and properly addressing cases at higher risk for ectasia. Clinical decisions should be taken based not only on scientific evidence[6] but also should include individual practice experience and judgment. Much has been written about the role of corneal topography and central corneal thickness (CCT),[7–9] as the standard methods for screening refractive patients. Considering such classic criteria, the ectasia risk scoring system (ERSS) was developed by Randleman et al.[10] The ERSS was developed based on a retrospective case-control study, which evaluated Placido disc-based corneal topography, CCT, the level of correction, residual stromal bed (RSB), and patient's age. In this study, abnormal preoperative topography and age were the most significant predictive variables. The scoring method was validated by a second study with an incidence of 6% of false positives, if considering each eye as an isolated candidate.[11] However, if we consider that if one eye is excluded, then both eyes from the same patient would be excluded, the correct false positive ratio would be 11.6%. This may be conservatively acceptable for most surgeons, considering the severe nature of keratectasia. However, the most important limitation of the ERSS is related to the lack of proper sensitivity. The ERSS had 4% to 8% of false negatives in the original studies,[10,11] and a separate retrospective study involving 36 cases with ectasia after LASIK found 9 eyes (25%) classified as low risk and 7 eyes (19%) as moderate risk.[12] In addition, a much higher incidence of false positives may be encountered, mostly if a younger population of LASIK candidates with normal topographies is evaluated.[13,14] The relatively high incidence of false negatives on the ERSS goes in agreement with other reported cases of ectasia after LASIK in the absence of apparent risk factors.[15–18]

Considering the limitations of the standard screening methodology, there is an unquestionable need for novel diagnostic tools that will complement front surface curvature map (topography) and CCT for developing a more sensitive and specific approach for identifying ectasia risk among refractive candidates.[19]

■ The Concept of Enhanced Screening for Detecting Ectasia Susceptibility

The best predictor for the development of ectasia after LASIK is the presence of an overlooked ectatic disorder preoperatively,[4,12,20,21] in which LASIK is an aggravating factor for the acceleration of the ectatic process. However, ectasia may also occur in an otherwise healthy cornea if there is significant weakening caused by the surgery.[5] This can be related to a thick flap and/or excessive tissue removal because of high corrections[22] or retreatments.[23] In either situation, biomechanical failure occurs because the RSB is not enough for maintaining corneal strength after the procedure. A lower limit RSB of 250 µm has been commonly deemed acceptable,[6,24] but a limit of half of corneal central thickness seems more appropriate.[9] However, there are cases with RSB higher than 250 µm that developed ectasia,[17,25,26] whereas there are cases with RSB even lower than 200 µm that remained stable with long follow-up.[27] In addition, ectasia can also occur after surface ablation procedures,[28,29] although the biomechanical impact of the ablation on the anterior stroma is much less pronounced if there is no lamellar cut.[30] Interestingly, a series of ultrathin corneas after therapeutic surface ablation with long-term stability was described by Vinciguerra et al.[31]

Thereby, the limits for a safe and stable RSB vary significantly among each individual cornea. The individualized level of susceptibility or predisposition for developing ectasia should be the ultimate goal when screening LASIK candidates. Since 2004, we have routinely performed 3-dimensional corneal tomography and biomechanical analysis using the Pentacam Corneal Tomographer (Oculus GmbH, Wetzlar, Germany) and the Ocular Response Analyzer (ORA, Reichert Ophthalmic Instruments, Buffalo, NY), respectively, for screening refractive candidates (Ambrósio Jr R et al Clinical Evidence of the Enhanced Sensitivity and Specificity of Corneal Tomography and Biomechanics for Screening Ectasia in Refractive Candidates ePoster ASCRS 2009. http://ascrs2009.abstractsnet.com/acover.wcs?entryid=000161).

■ A Critical Revision on "Topospeaking"

"Topography" derives from Greek words "to place" (topo) and "to write" (graphein), which means to describe a place. The term "corneal topography" has been classically used for the reconstruction of the front (anterior) corneal surface, which is commonly achieved by reflective, Placido disc-based systems. Corneal topography represented a true revolution in the diagnosis and management of corneal disease[1] and has a recognized role in the development of refractive surgery.[7,32,33]

The term "tomography" was also derived from the Greek, as the combination of "to cut or section" (tomos) and "to write" (graphein).

Corneal tomography is related to a 3-dimensional reconstruction of the cornea and should be used for the characterization of the elevation of the front and back surfaces of the cornea, along with pachymetric mapping. Different technologies such as horizontal slit scanning, rotational Scheimpflug, arc scanning with very high-frequency ultrasound, and optical coherence tomography are available in many commercial instruments.[34]

Corneal topography was found to be sensitive for detecting subtle (subclinical) changes on the anterior corneal surface secondary to ectatic disorders before loss of best spectacle-corrected visual acuity and the development of typical slit-lamp biomicroscopy findings (Figs. 1–3—OD).[35,36] The occurrence of subclinical cases of keratoconus represent an unquestionable argument for topography to be considered as a critical test before any refractive procedure. However, there are cases with topographic similarities of ectasia on the curvature map that may not represent true ectatic disease, which may be related to abnormal ocular surface such as in anterior basement membrane dystrophy (Fig. 4), contact-lens warpage,[37] or simply a rare variation of normality.[38]

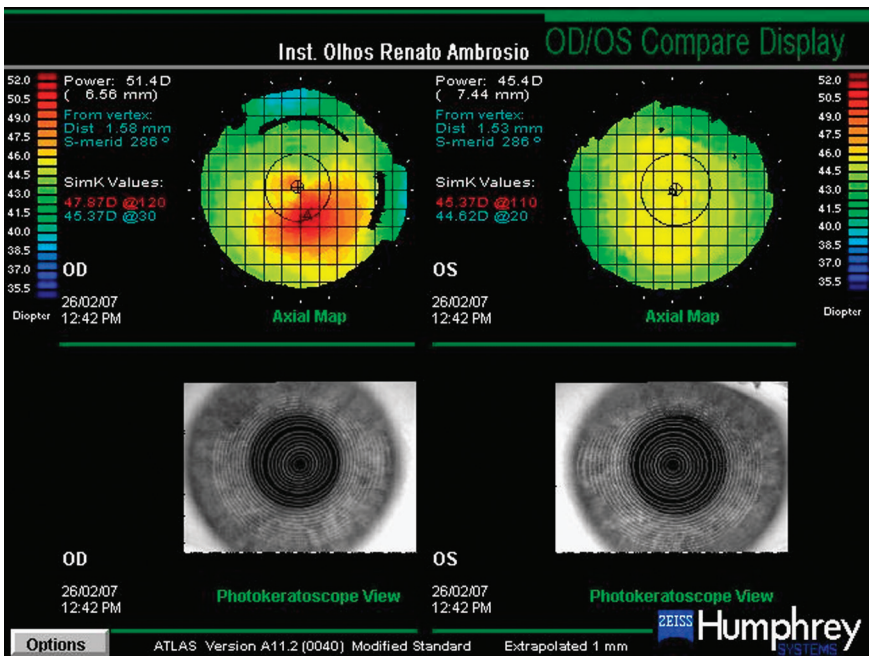

Figure 1. *Axial curvature map and photokeratoscopic image from Placido disk-based corneal topography acquired from ATLAS (Zeiss Humphrey, San Leandro, CA) taken for a 20-years-old male patient with very asymmetric keratoconus. UCVA was 20/100 in OD and 20/200 in OS. BSCVA is 20/20-1 in OD and 20/15 in OS with + 0.25 -3.25 × 79° in the right eye and -1.00 -0.50 × 126° in the left eye. Slit-lamp corneal examination was unremarkably normal unless for more evident corneal nerves in the mid stroma in both eyes. (same eyes as in Figs. 2, 3)*

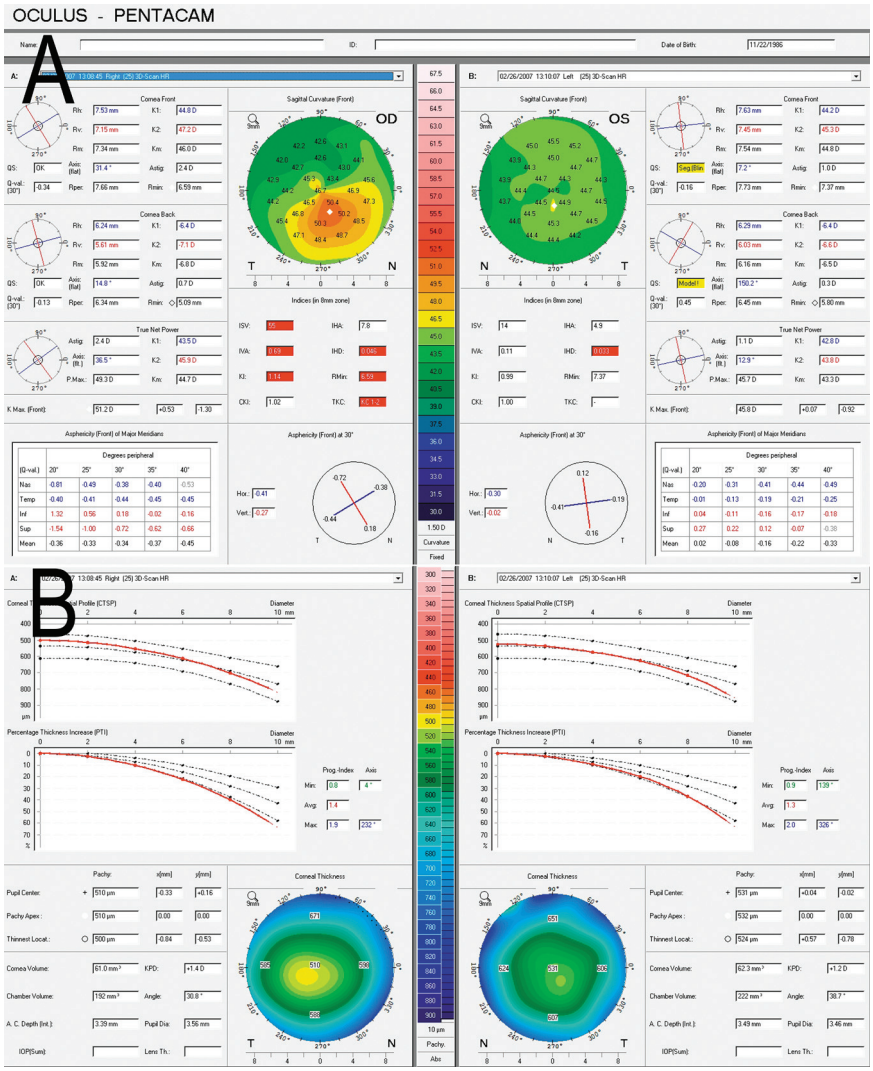

Figure 2. *Corneal curvature (sagittal or axial) taken from the Pentacam HR (Oculus) from the same eye as in Figure 1 and 3. The topometric artificial intelligence based on front surface curvature data at 8 mm indicates KC 1 to 2 in OD and normal pattern in OS. The corneal thickness spatial profile and percentage thickness increase graphs show an abnormal thickness profile despite normal central corneal thickness of 510 and 531 μm in OD and OS, respectively. Note the Ambrósio relational thickness maximal of 268 μm [thinnest point (TP) = 500; pachymetric progression index (PPI) Max = 1.9] in OD and 262 μm (TP = 524; PPI Max = 2) in OS.*

Other cases with mild irregularities, which do not meet the criteria for keratoconus, are defined as keratoconus suspects (KCS) (Fig. 5A). Compared with topography (anterior curvature), tomographic analysis has proven effective for enhancing specificity among such cases (Fig. 5B).

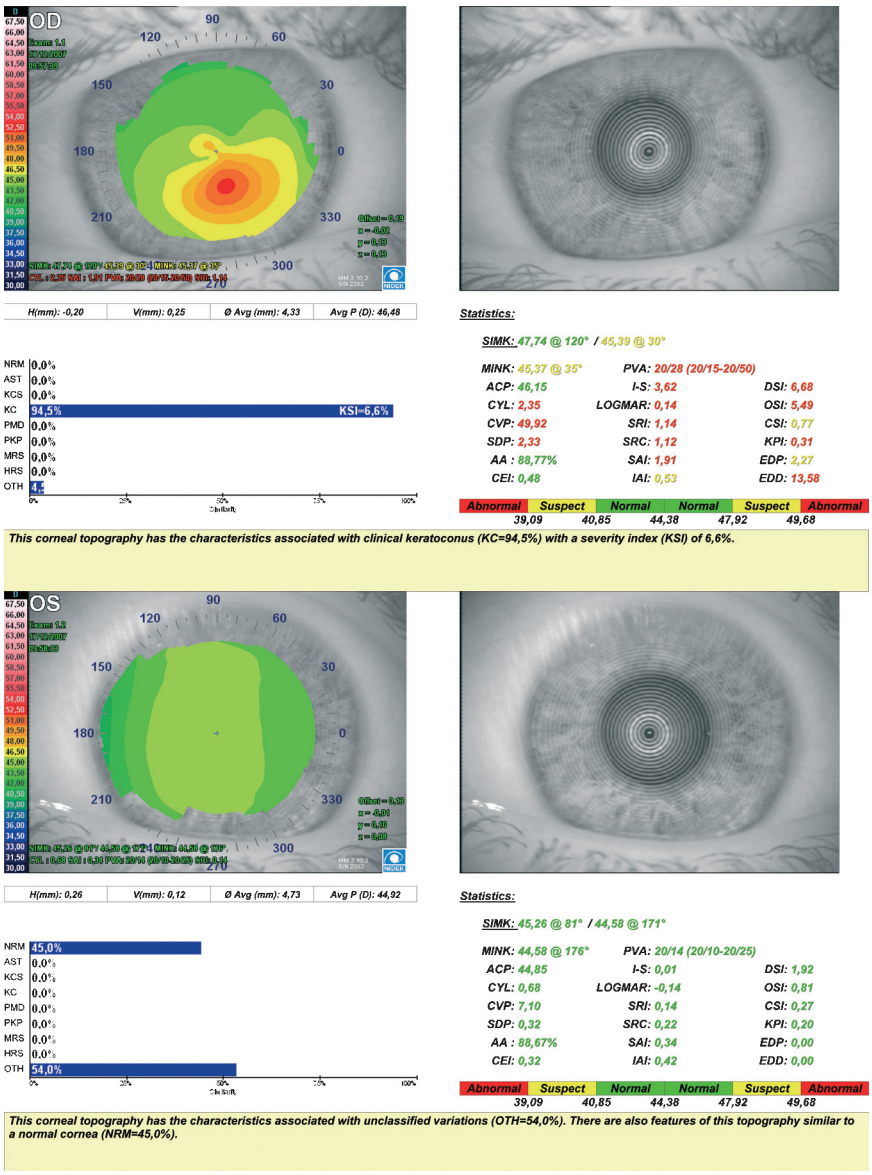

Figure 3. *Axial Curvature Map, photokeratoscopic image, and artificial intelligence system (Nidek Corneal Navigator) acquired from Nidek Magellan (Gamagori, Japan). Note similar findings as in Figures 1 and 2. OD has 94.5% similarity with KC (KSI 6.6%), whereas OS has 45% of similarity with a normal pattern and 54% of similarity with unspecific pattern.*

More importantly, there are circumstances in which the ectatic change is not yet present on the front surface, so that corneal topography seems to be normal despite subtle disease. Such special groups of cases include the

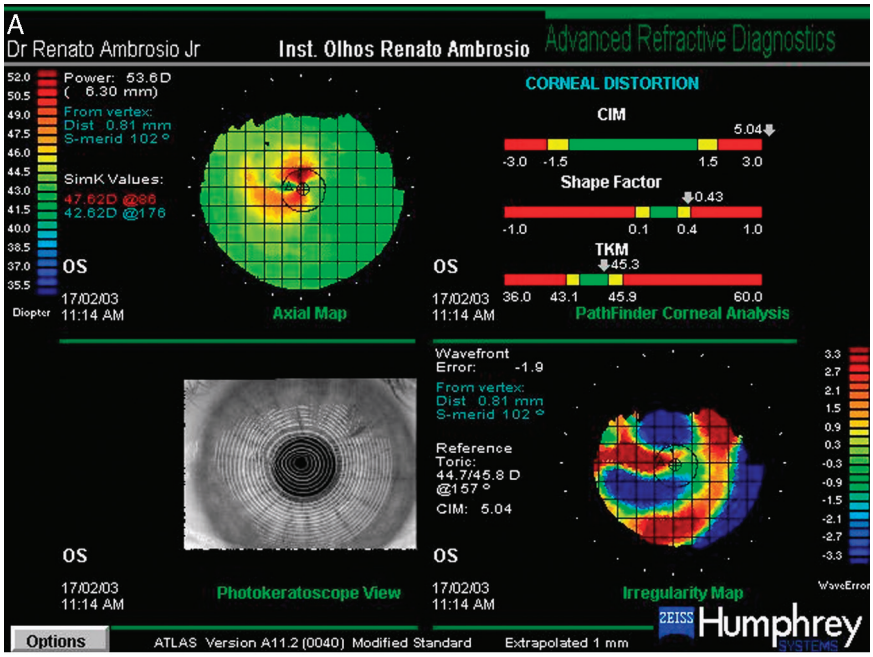

Figure 4. *A, Corneal Topography from a case with false ectasia because of irregular surface. Note the central area with more than 50 D, which coincides with the irregular photokeratoscopic reflex. B, Slit-lamp biomicroscopy showing classic fingerprinting on the epithelium related to anterior basement membrane dystrophy.*

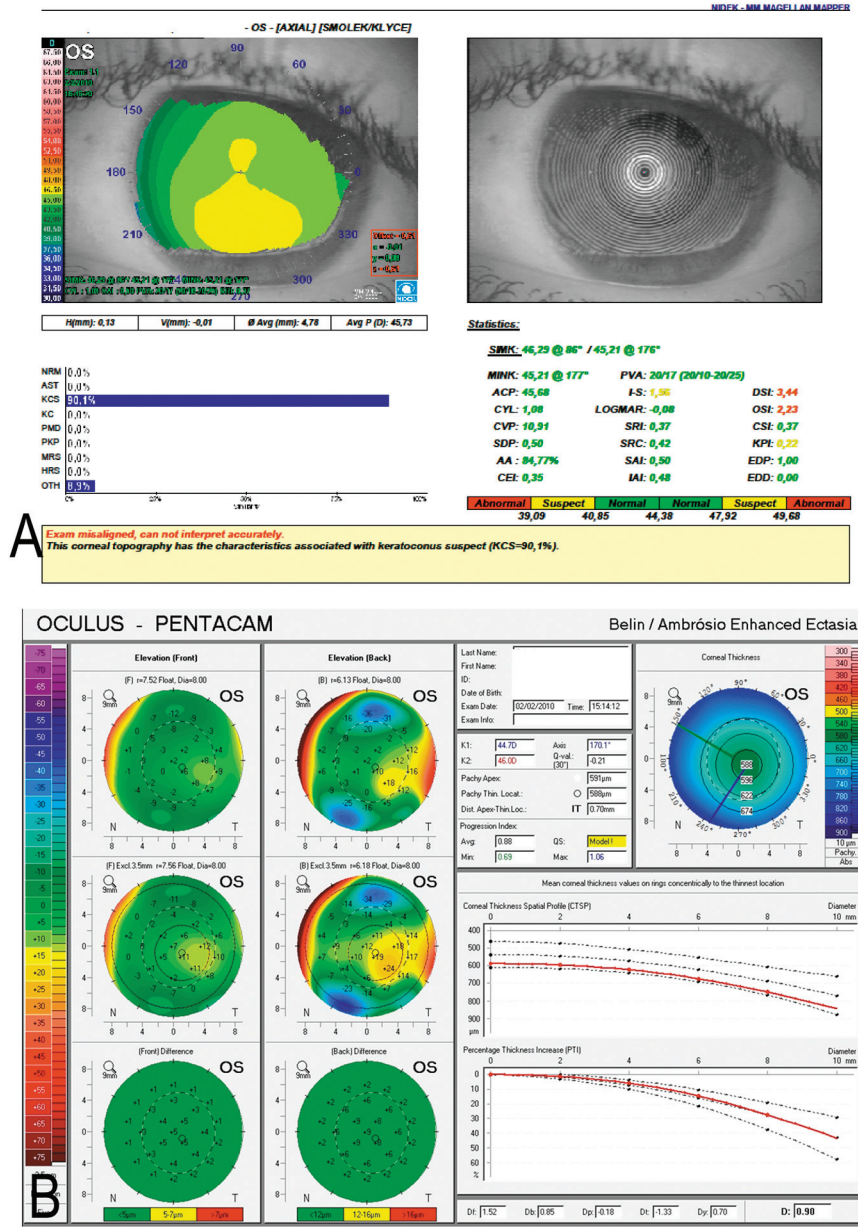

Figure 5. *A, Corneal topography findings from Nidek Magellan and (B) Belin-Ambrósio Enhanced Ectasia Display from Oculus Pentacam of a case with inferior steepening but no evidence of ectasia on clinical examination. Note 90.1% of similarity with a KCS pattern at the Nidek Corneal Navigator, while the tomographic data show a thick cornea (central corneal thickness = 591 μm) with normal pachymetric distribution and normal elevation findings from the front and back corneal surfaces. Same eye as in Figure 16, which shows normal biomechanical properties.*

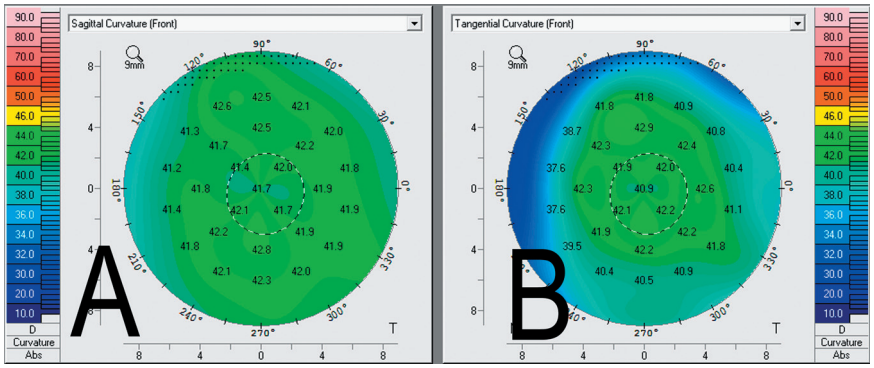

Figure 6. *Sagittal (A) and Tangential (B) curvature maps from the Pentacam using the Ambrósio-2 scale. Note the tangential map evidences more irregularity pattern, but there is no definitive evidence of abnormality. The contralateral eye of this patient has clinical keratoconus.*

contralateral eyes with normal topographies from patients with very asymmetric (not truly unilateral) keratoconus (Figs 1–3—OS, Fig. 7), [39–43] and cases with natural progression of keratoconus which have been documen-

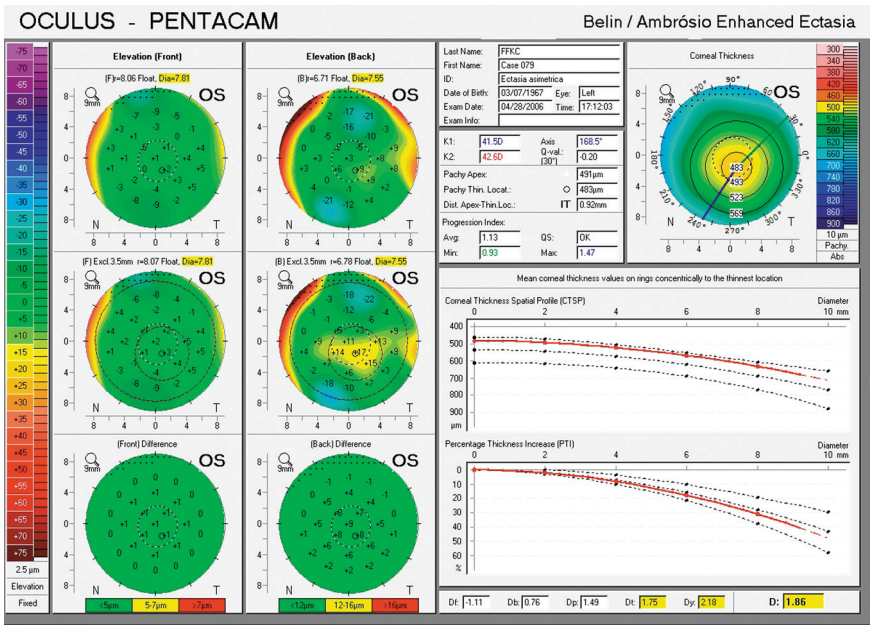

Figure 7. *Belin-Ambrósio enhanced ectasia display from Oculus Pentacam of the same eye as in Figures 1 and 2. Note the final D value of 1.86, Ambrósio relational thickness maximal of 327 µm (thinnest point = 483; pachymetric progression index Max = 1.47), which is consistent with high ectasia susceptibility. Clinical examination was unremarkable and BSCVA was 20/15 with mild myopic astigmatism.*

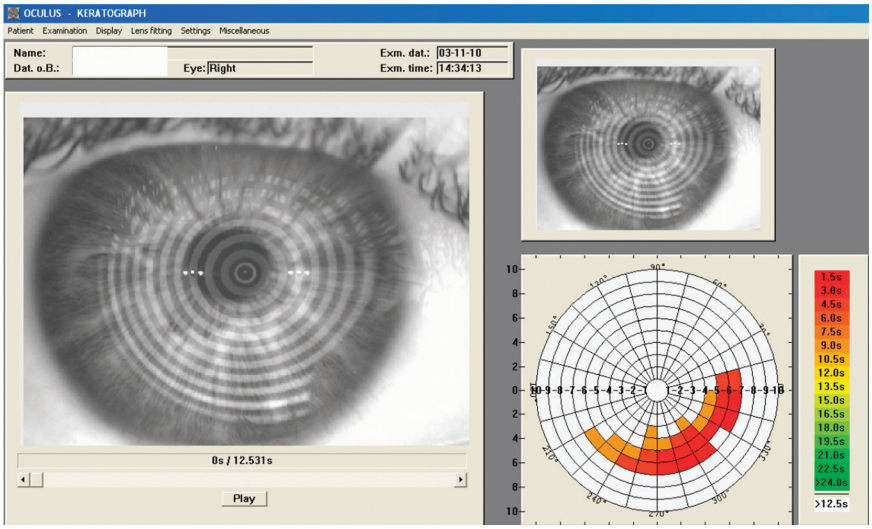

Figure 8. *Noninvasive break-up timb (BUT) display from the Oculus Keratograph. Note the localization of the area with faster BUT (<5 s) within the inferior paracentral area.*

ted earlier have normal anterior curvature examinations. These subclinical cases with normal topography represent an opportunity to test the sensitivity of novel examinations to detect milder forms of ectasia (Fig. 2B, Fig. 7). We refer to such cases as with high susceptibility or predisposition to develop ectasia, but they may be also referred as forme fruste keratoconus—a term introduced by Amsler in 1961[44] that is still widely used.[39,42,45,46] The identification of such very subtle abnormalities should be the goal of the enhanced screening of ectasia risk among LASIK candidates, as the referred ectasia susceptibility condition would be likely present in the preoperative state of cases with unexplained ectasia after LASIK.[17]

Finally, it is critical to recognize that the topographic diagnosis of KCS does not always imply a true form of ectasia (Figs. 5, 6), whereas ectasia susceptibility or forme fruste keratoconus, a pretopographical form of the condition, may occur despite of a normal topography and CCT (Figs 1–3—OS, Fig. 7). In addition, the differences between corneal topography and tomography should be accepted, so that authors will adhere to proper terminology. Both technologies will coexist and are complementary.[47] For example, although tomography allows for the evaluation of the posterior (back surface) elevation and pachymetric mapping, which enhances the sensitivity to detect more subtle ectatic abnormalities before front curvature changes,[17,42] Placido reflection topography enables the evaluation of the tear film, which is also relevant for screening risk for dry eye after LASIK (Fig. 8).[48]

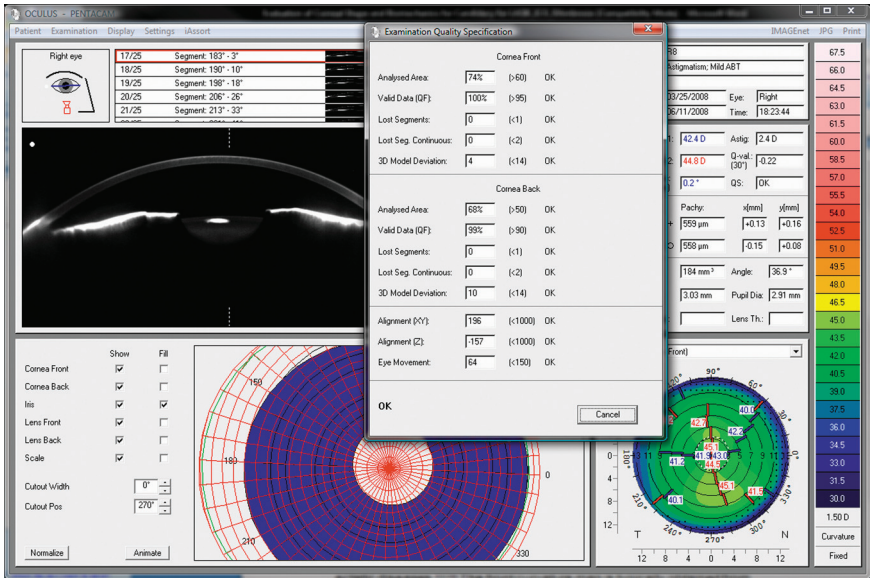

Figure 9. *Pentacam quality score display.*

■ Guidelines for the Evaluation of Corneal Shape

Appropriate interpretation of color-coded topographic and tomographic maps is a relatively complex task that may be difficult and confusing for many clinicians. There are important considerations that should be taken for a correct interpretation of the data obtained from such examinations. The first critical point is that any map should be considered valid only if the raw data on which it is based is confirmed as reliable. For example, in Placido disc-based examinations, it is important to evaluate the videokeratoscope image, so that proper centration is evaluated along with the quality of the mires (Figs. 1,3, Fig. 5A). In some instruments, such as the Pentacam, a quality score was developed (Fig. 9), so that the clinician can immediately determine, objectively, whether the examination is reliable.

The clinician should also recognize the type of map that is evaluated along with the color-coded scale. The number of colors, the steps between each color, the highest and lowest colors, and the grading change between each color are the main characteristic to be considered. Normalized or variable scales adjust to each examined eye, which, in conjunction with a smaller step between each color, would increase the sensitivity for detecting irregularities. Absolute fixed scales offer the advantage of standardizing color recognition for particular values.[49,50] Thereby, this is critical that each examiner knowingly decides which

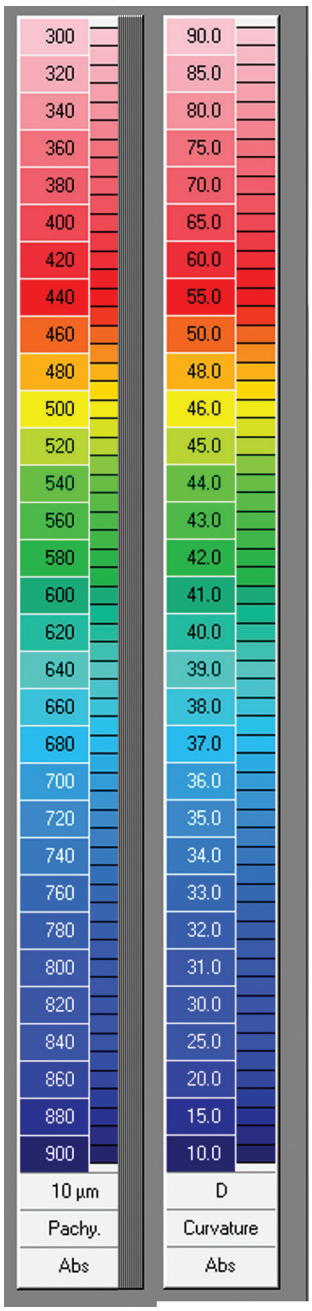

Figure 10. *Ambrósio-2 color scale for pachymetric and curvature maps.*

color-coded scale will be used so that proper interpretation will be facilitated.

An absolute scale has been developed for curvature and pachymetric maps (Fig. 10). This scale, named "Ambrósio 2," is available on the Pentacam software. This scale should always be used with 61 colors and absolute values, as the values obtained will be in accordance with studies comprising 226 normal corneas, 34 corneas with Fuchs endothelial dystrophy, and 88 keratoconic corneas (Ambrósio, Caiado, and Bonfadini, unpublished data 2009). For sagittal curvature maps, in a normal population, the average central keratometry (K) was 43.1 ± 1.43 D (SD) and the average for highest K (KMax) was 44.6 ± 3.4 D (SD). These values were included on the range of green to green-blue on the color-coded scale. Interestingly, the best cutoff value for KMax in the receiver operating characteristic (ROC) curve was 47.9 D (sensitivity of 97.7% and specificity of 96.9%), so that 48 D was set for the orange to red transition. Considering thickness maps, mean thinnest point (TP) value in the normal population was approximately 550 µm and standard deviation (SD) of 30 µm. Then, the green color was centered on the 550 and the shades of darker and lighter green were calculated to be within 1 SD. The best cutoff value in the ROC curve for keratoconus and normals was around 500 µm (sensitivity of 87% and specificity of 90%), which was set for the yellow threshold. On the thicker side, mean TP value for Fuchs corneas and the best cutoff value in the ROC curve was 625 µm (sensitivity of 82% and specificity of 91%), which was set for the threshold of green to blue.

Curvature Maps

It is also critical that the examiner understands the fundamentals for the reconstruction of the maps. Many algorithms can be used for curvature, refractive, and power keratometric maps. Basically, there are 2 types of maps that are commonly used in curvature maps that are relevant for ectasia screening: sagittal (or axial) maps and tangential (or instantaneous) maps. In sagittal maps [Figs. 1–3, Fig. 5A, Fig. 6A (left map), Fig. 7A (left map)], corneal curvature is determined at each measured points at a normal (90 degrees) angle to its surface, referenced to the mid line or measurement axis. Tangential maps evaluate the local radius of curvature at each measured point, which is more sensitive to detect irregularities [Fig. 6A, Fig. 7A (right maps)]. Importantly, classic screening systems such as the Rabinowitz-McDonnell were developed based on axial maps. These indices are based on the steepness of the cornea (suspicious when higher than 47.2 D), and superior-inferior asymmetry (suspicious when higher than 1.4 D).[51] Topographic indices and artificial intelligence systems have been developed to facilitate clinical interpretation (Fig. 2A, Fig. 3, Fig. 5A),[52,53] but this is very important for the clinician to understand their basics and

limitations and to be able to identify the normal curvature patterns[38] and the ones described in ectatic diseases.[51,54–58]

Elevation Maps

The first critical consideration for elevation maps is to understand that these maps represent the difference from the examined corneal surface (anterior or posterior) compared with a chosen reference body.[59] Typically, the reference is calculated to have more coincident points (best fit) with the examined surface. Float and shift optimization functions are also used to improve the number of coincident points of the selected reference and the examined surface. Different areas of the examined corneal surface can be considered for the calculation, producing different best-fit references. For example, in a normal prolate cornea (steeper in the center and flatter in the periphery), if a larger area is considered for calculating the best-fit sphere (BFS), a flatter reference would be chosen, which would exaggerates elevation values (Fig. 11). For practical purposes, our preference for screening for ectasia is to fix to the 8 mm zone for calculating the BFS, as this zone is available for the majority of examined eyes. The shape and the values on elevation maps should be evaluated in conjunction.[59] The elevation values at the apex, at the TP,[60] and the maximum value above the BFS within the central area[61] can be used.

Different geometric bodies can be used for serving as reference for the elevation map, such as spheres, ellipsoids, and toric ellipsoids. It is important that the examiner understands the impact of selecting different geometric bodies along with the zone diameter to calculate the

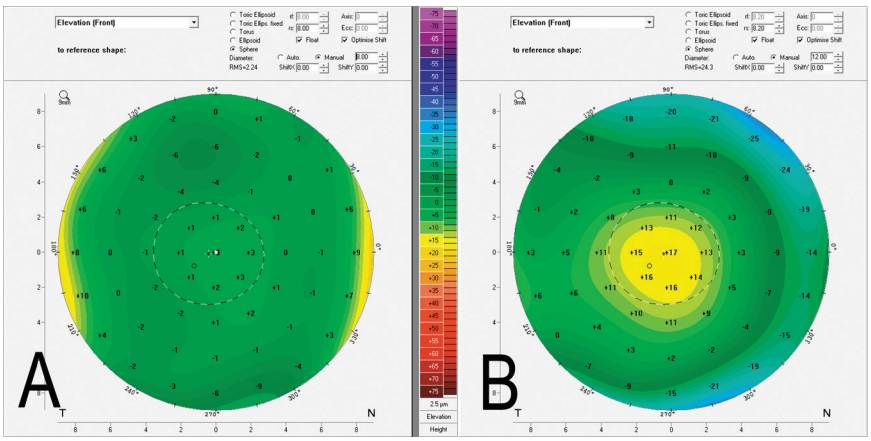

Figure 11. *Impact of the zone diameter for calculating the best-fit sphere (BFS) in a normal cornea. Note the normal pattern with the BFS for the 8-mm zone (A) and the protrusion appearance because of the flatter BFS (8.2 mm) with the 12-mm zone (B).*

best fit. For example, the BFS allows for the identification of astigmatism, whereas the best-fit toric ellipsoid (BFTE) facilitates the evaluation of higher order astigmatism. Interestingly, we found similar performances for the elevation values at the TP of the posterior surface using BFS and BFTE (8-mm zone) in a study comprising 100 normal corneas (50 patients) and 60 keratoconic corneas (30 patients). The best cutoff for the BFS was 19 μm with an area under the ROC (AUROC) of 0.98; for BFTE, the best cutoff was 12 with AUROC of 0.97 (Canedo, Louzada, Belin, and Ambrósio, unpublished data 2009).

The Belin Intuitive Scale with 61 colors and 2.5 μm step (Fig. 12) has been found to be the most reliable for elevation maps. For example, in normal eyes, average elevation value at the TP using a floated BFS for 8.0 mm is 3.6 ± 4.7 μm,[55,60] so that the yellow value of + 15 at the TP indicates this is suspicious and would occur in less than 1% of normal corneas.

The "enhanced reference surface" concept was introduced by Michael W. Belin, MD. This approach was designed to highlight the ectatic area on the elevation map by excluding an area centered on the thinnest portion of the cornea from the BFS calculation. If the excluded area is more protruded, the resultant BFS would be flatter and the cone or ectatic region would be more pronounced. Different exclusion zone diameters and centers were tested in a preliminary study (Salomão, Ambrósio, Belin, unpublished data 2008). The most reliable enhanced reference was computed by determining the BFS for the 8.0-mm zone after excluding all the data from a 3.5-mm zone centered on the TP of the cornea. The subtraction map of the standard BFS elevation from the "enhanced elevation" detects and highlights the protrusion area and has been shown to be a key differentiator between normal and ectatic corneas. This approach is used for the anterior (front) and posterior (back) elevation. Normal population studies were carried out, serving as the basis for the "green-yellow-red" color thresholds that are encountered on the Belin-Ambrósio enhanced ectasia display (BAD) on the Pentacam software.

Thickness Maps

Corneal tomography provides data for the reconstruction of the pachymetric map. Along with the determination of the true TP value and its location in relation to the center of the cornea, thickness distribution throughout the entire cornea can be characterized. We have previously developed and described the graphical concept of a corneal thickness spatial profile (CTSP) and percentage thickness increase (PTI).[62–64] Starting from the TP outward, the CTSP describes the rate of increase of corneal thickness using the average of pachymetric values within annular rings concentric to the TP separated by 0.1 mm

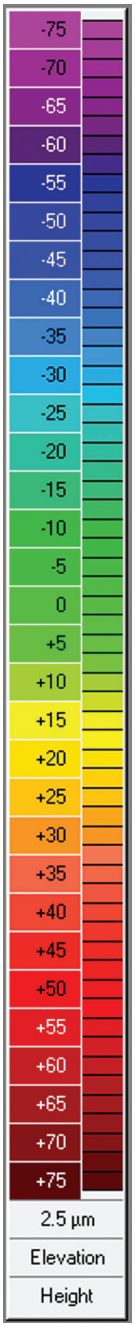

Figure 12. *Belin intuitive elevation scale.*

steps. The PTI involves a similar measuring process centered on the TP, but it takes the percentage of thickness increase from the TP for the average along each ring. The Pentacam (Oculus GmbH) software reports CTSP and PTI of the examined cornea in graphs along with the data of the mean and 2 standard deviations of a normal population (Fig. 13). From these data, pachymetric progression indexes (PPIs) are calculated for all hemimeridia over the entire 360 degrees of the cornea, starting from the TP. The average of all meridia is noted as the pachymetric progression average (PPI Ave) and the meridians with maximal (PPI Max) and minimal (PPI Min) pachymetric increase are noted along with their axes (Fig. 13, progression index box). In a normal population, the averages and SD of PPI of the minimal meridians, maximal meridians, and average of all meridians are 0.58 ± 0.3, 0.85 ± 0.18, and 0.13 ± 0.33, respectively. The pachymetric index will be higher if the cornea gets thicker in a more accelerated pattern from the TP out to the periphery (PTI and CTSP graphs falling down).

The best parameter for diagnosing keratoconus is the "relational" thickness, which is the thinnest pachymetric value divided by the pachymetric progression. The"Ambrósio relational thickness" (ART) may be calculated for the minimal (ART-Min), average (ART-Mid), and

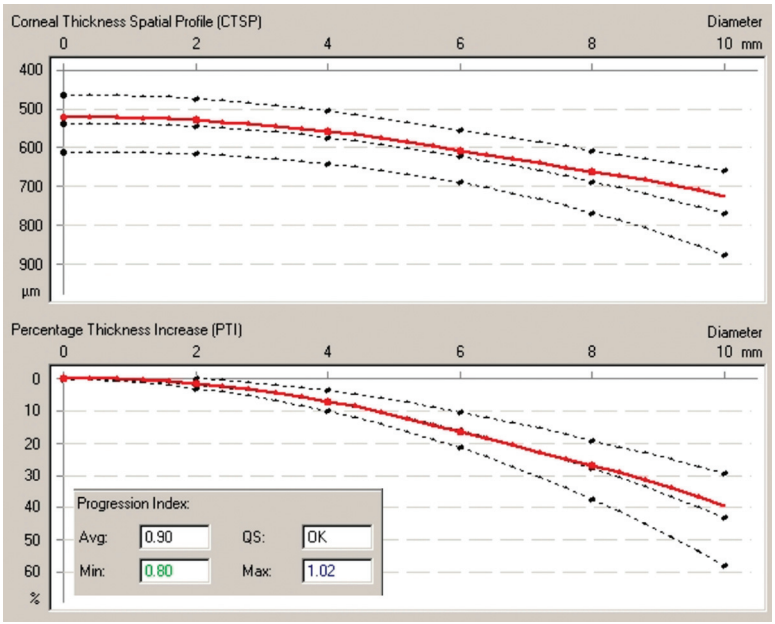

Figure 13. *Pentacam pachymetric display of a normal cornea with average central corneal thickness.*

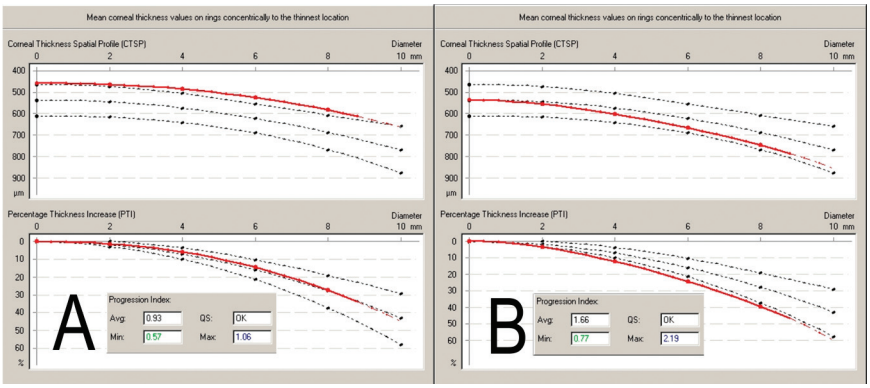

Figure 14. *Corneal thickness spatial profile and percentage thickness increase graphs of a normal thin cornea (A) and one with keratoconus with normal central thickness (B). Central corneal thickness and thinnest point for the normal thin cornea are 458 and 457 µm and for the keratoconic cornea, 536 and 545 µm. Ambrósio relational thickness maximal is 431 µm for the normal thin cornea and 245 µm of the keratoconic cornea.*

maximal values (ART-Max). The ART-Mid and ART-Max have AUROC of 0.98 and 0.99, with cutoffs of 426 and 339 µm, respectively, for diagnosing keratoconus (n = 88) from normals (n = 226) (Ambrósio, Guerra, Caiado, and Belin, unpublished data 2010). This approach enables the recognition of a normal thin cornea (Fig. 14A) and one with keratoconus with relatively normal CCT (Fig. 14B).

The Belin-Ambrósio Enhanced Ectasia Display

The BAD combines elevation-based and pachymetric evaluations in 1 comprehensive display to give the clinician a global view of the tomographic structure of the cornea. Deviation of normality values were implemented for the front (df) and back (db) enhanced elevations, thinnest value (dt), pachymetric distribution (dp), and vertical displacement of the thinnest in relation to the apex (dy) (Figs. 5B, 6B, 7B). The "d" values are calculated so that a value of zero represents the average of the normal population and 1 represents the value is one standard deviation toward the disease (ectasia) value. A final "D" is calculated from a regression analysis that weights differently each parameter. Each parameter is indicated in yellow (suspicious) when it is $\geq$1.6 SD from the mean and turns red (abnormal) at $\geq$2.6 SD from the mean. Values below 1.6 SD are reported in white and are viewed as within the normal range.

In a study comprising 25 patients with very asymmetric keratoconus, BAD was sensitive to detect abnormalities in 24 of 25 (94%) of the contralateral eyes with no keratoconus pattern detected by corneal topography (anterior curvature). The final D was the best parameter with a cutoff of 1.27, followed by ART-Max with a cutoff of 391 µm.

These values are in agreement with other cases with ectatic progression after LASIK despite no detectable risk factors.

■ Corneal Biomechanics

The need for an advanced understanding of corneal biomechanical properties is further highlighted by cases of ectasia despite what are normal preoperative examinations. The relevance of corneal biomechanics for refractive surgery goes beyond ectasia prevention, however, as this variable also has the potential to improve outcomes in refractive surgery,[65] not to mention the ability to correctly evaluate IOP which is severely affected by corneal surgery.[66] The January, 2005 (Volume 31, Issue 1) special issue on corneal biomechanics of the *Journal of Cataract and Refractive Surgery*, guest edited by Dr Cynthia Roberts, PhD, introduced the concept of "Biomechanical customization" in refractive surgery.[67]

However, until the commercial introduction of the Ocular Response Analyzer[66] (ORA, Reichert Inc., Depew, NY) in the 2005 European Society of Cataract and Refractive Surgery meeting (Lisbon, Portugal), corneal biomechanical evaluations were limited to laboratory in vitro studies and to virtual mathematical corneal finite element models.[68,69] The ORA is a noncontact tonometry, which was designed to provide a more accurate measurement of IOP through the understanding of corneal properties. The ORA has a precisely metered collimated air pulse and a quantitative electro-optical system that monitors the deformation of the cornea through the corneal reflex of an infrared light. The measurement takes approximately 20 milliseconds. After autoalignment to corneal apex, the air puff starts. The air pump is controlled accordingly to the first applanation signal, when there is an internal command on the instrument for the air pump to shut off so that the decrease phase is symmetric to the increase phase. The air pressure forces the cornea to deform inward, passing first applanation, when the pressure (P1) is registered. The cornea goes into a slight concavity until the air pump shuts off so that the cornea will gradually recover to its normal configuration, passing through a second applanation (P2) state. The applanation events are registered by a peak on the corneal reflex signal (red curve, Fig. 15), so that two independent pressure values are registered. The pressure measurements (P1 and P2) serve as the basis for the variables reported by the original ORA software (Table 1). The difference between the 2 pressures is called corneal hysteresis (CH), which was the new concept introduced to the Ophthalmic community.[70] The term hysteresis is derived from the Greek word meaning "lagging behind" (http://en.wikipedia.org/wiki/Hysteresis). CH and corneal resistance factor (CRF) have a positive statistically significant relation with

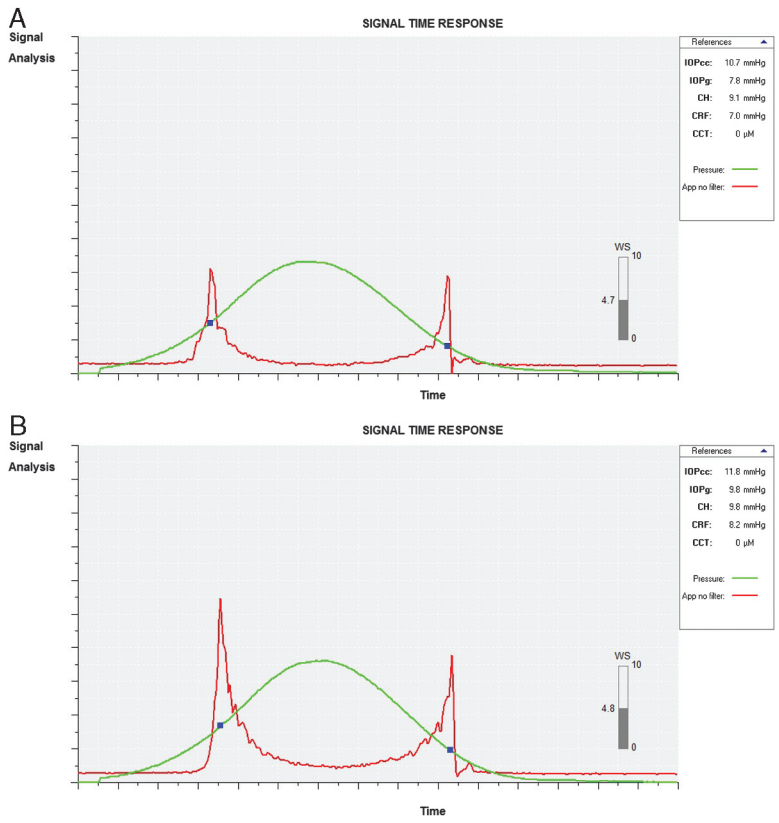

Figure 15. *Ocular response analyzer findings from the same case as in Figures 1 to 3. Note corneal resistance factor of 7.0 and 8.2 mm Hg in OD and OS, respectively.*

CCT (CH, $r = 0.4655$; CRF, $r = 0.5760$).[66,71] CH and CRF are also statistically lower in keratoconus (Table 1)[40,72,73] and also decreased after LASIK and surface ablation procedures.[74–77] No associations were found between CRF nor CH and simulated keratometry, anterior chamber depth or spherical equivalent refraction.[71] Paradoxically there is a negative correlation between CH and CRF and age,[71] while there is an expected considerable increase in the values of the modulus of elasticity and age accordingly to human corneal inflation studies.[78]

In a study comprising 226 normals and 88 keratoconic eyes, the ROC curves for CH and CRF found cutoffs of 9.4 mm Hg and 8.1 mm Hg, respectively. However, there is a significant overlap for the distribution of these metrics in normal cases and keratoconus cases. For CH, the sensitivity and specificity were 0.816 and 0.721, respectively, whereas for CRF the sensitivity and specificity were 0.79 and 0.854, respectively (Ambrósio, Fontes, Bonfadim, and Canedo, unpublished data 2009).

Table 1. *Original Reichert Ocular Response Analyzer Parameters (Canedo, Bonfadin, Fontes, and Ambrósio, Unpublished Data 2009)*

Variables (all Measurements in mm Hg)	Formula	Mean in Normal (n = 226)	SD	Mean in Kerato-conus (n = 88)	SD	Mann-Whitney Test
"Gold standard" calibrated IOP	(P1 + P2)/2	14.82	3.56	11.20	6.41	<0.001
Corneal compensated IOP	(P2 – 0.43 × P1)	15.38	3.49	14.60	5.83	0.2
Corneal hysteresis	(P1 – P2)	10.41	1.74	8.24	1.82	<0.001
Corneal resistance factor	(P1 – 0.7 × P2)	10.23	1.88	7.29	2.5	<0.001

IOP indicates intraocular pressure; P1, first applanation; P2, second applanation.

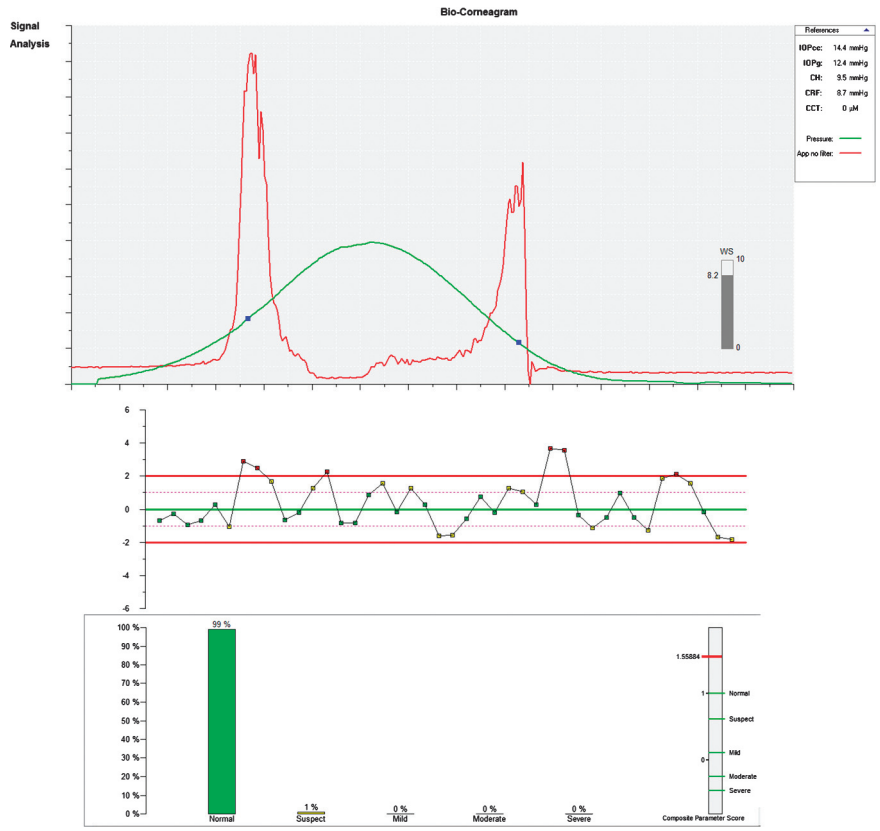

Figure 16. *Ocular response analyzer advanced analysis from the same case as in Figure 5, which evidences enhanced specificity for detecting a normal pattern along with the tomographic data. Note the 99% similarity with a normal pattern.*

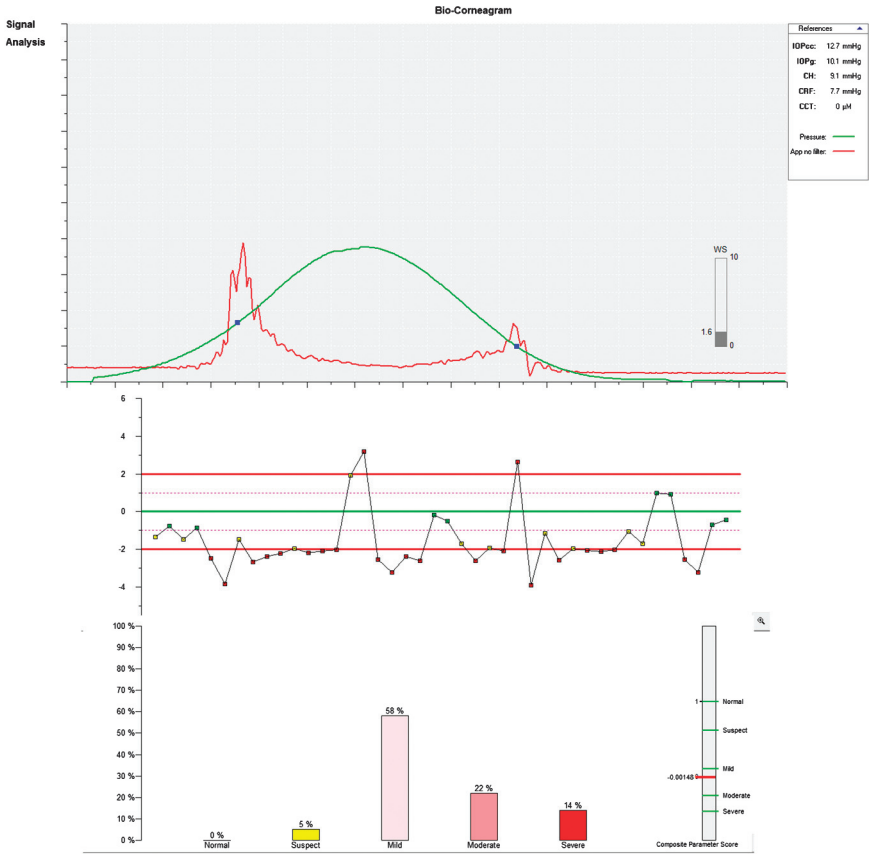

Figure 17. *Advanced ocular response analyzer analysis of a mild keratoconus (same eye as in Fig. 14B). Note the lower peaks in the waveform signal and the higher percentage of a keratoconic pattern.*

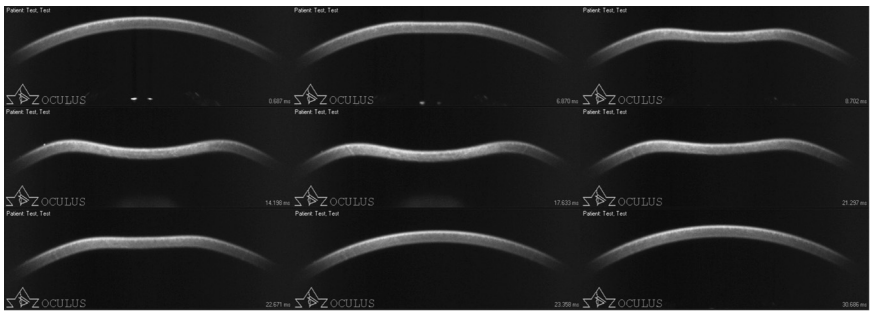

Figure 18. *Dynamic Scheimpflug images taken from the CorVis ST of a normal eye. Note the complete visualization of the deformation process in relation to the time frame. Examination takes less than 20 min.*

Interestingly, "gold standard" IOP but not corneal compensated IOP was found statistically different among keratoconus and normals (Table 1).

In addition to the "classic" ORA parameters, CH and CRF, a new set of 36 new waveform-derived parameters were studied. These parameters are basically related to specific waveform characteristics, such as the width, peak, area, and height of the peaks (signal during applanation moments), and general morphology of the waveforms (Luce, unpublished data 2008). Interestingly, there are cases with the same CH and highly different waveform signals and clinical characteristics. In fact, Kerautret and colleagues[79] reported a case of unilateral corneal ectasia after bilateral LASIK, in which CH and CRF were almost equal in both eyes while significant between-eye differences in the waveforms were

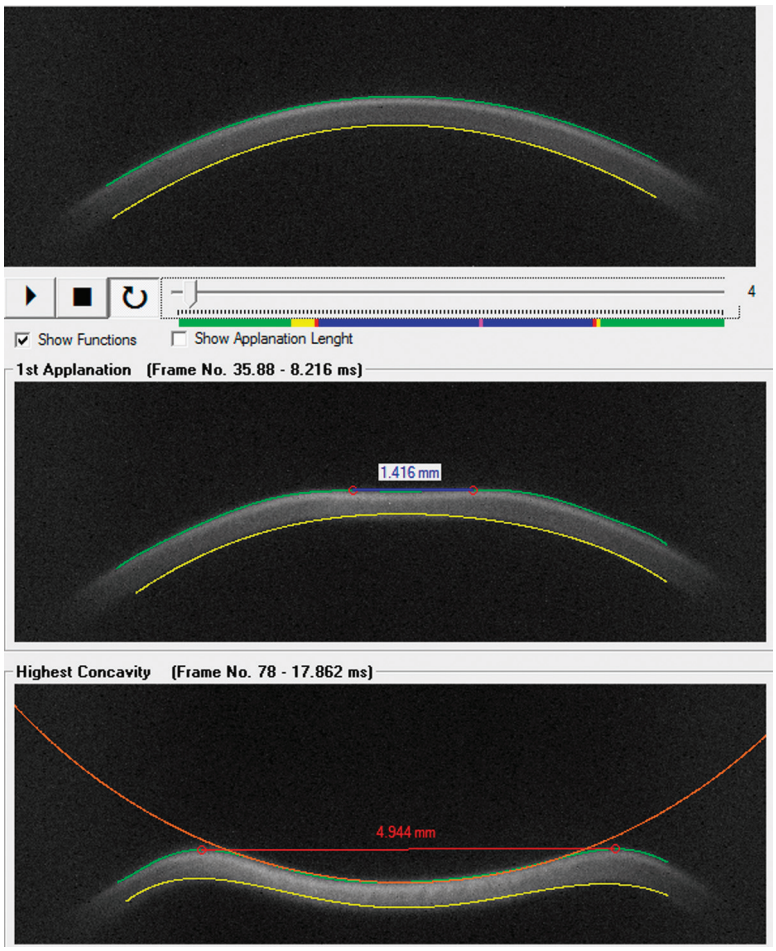

Figure 19. *CorVis ST display from a mild keratoconic cornea. Deformation amplitude is 1.15 mm*

noted, most prominently in the lower amplitude of the applanation peaks in the ectatic eye. In fact, we have learned to adopt such subjective analysis when evaluating the ORA signals in daily clinics. However, it is critical to provide objective metrics from these new parameters. It was found that a combination of the most relevant waveform-derived parameters would provide a better performance on the ROC curve. The new ORA display includes a table with all indices that are displayed as the deviation from normality and the keratoconus percentage similarity score (Figs. 16, 17). This approach has the potential to increase specificity of identifying a normal biomechanical signal in a case with a topographic KCS finding (Fig. 16), and confirming abnormal biomechanics in a mild keratoconus (Fig. 17).

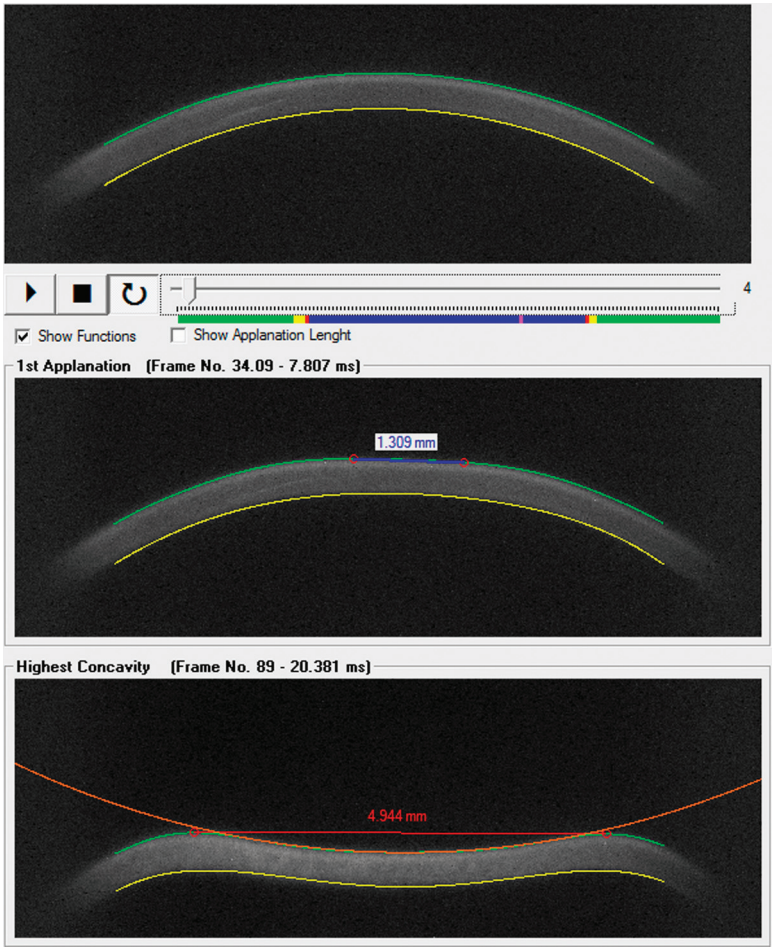

Figure 20. *CorVis ST display from a normal cornea. Deformation amplitude of 0.81 mm.*

A new noncontact tonometry system integrated with an ultra-high speed Scheimpflug camera was introduced by Oculus in 2010. The CorVis ST (Scheimpflug Technology) takes 4330 frames/sec covering 8 mm horizontally to monitor corneal response to a metered collimated air pulse with symmetrical configuration and fixed maximal internal pump pressure of 25 kPa. The addition of an ultra-high speed Scheimpflug camera allows dynamic inspection of the actual deformation process (Fig. 18), which has an enormous potential to provide further detailing for biomechanical characterization of the cornea and correct IOP readings. Preliminary results have found a statistically significant difference among keratoconic corneas and normals for many parameters, such as corneal speed during deformation, corneal applanation length, and deformation amplitude (highest displacement of the apex in the highest concavity momentum), which are important measures of corneal viscoelastic properties and stiffness (Figs. 19, 20). Current studies are being conducted for testing the performance of such parameters for assessing ectasia susceptibility among refractive candidates and to understand the impact of IOP on corneal deformation.

■ Conclusions

Screening for ectasia risk among LASIK candidates is one of the most important steps before LASIK. It is important to note that the goal is not only to identify cases with mild ectasia, but to characterize each cornea in terms of their risk or susceptibility to undergo biomechanical failure and ectasia. The standard screening criteria, based on corneal topography and CCT, has important limitations regarding sensitivity and specificity.[19] New technologies are needed and have already shown the potential for improving the sensitivity[46] and specificity[80] for detecting ectasia risk. However, there is still a need for retrospective case-control studies and, most importantly, prospective controlled studies which are being conducted.

■ References

1. Wilson SE, Ambrósio R. Computerized corneal topography and its importance to wavefront technology. *Cornea*. 2001;20:441–454.
2. Belin MW, Khachikian SS, McGhee CN, et al. New technology in corneal imaging. *Int Ophthalmol Clin*. 2010;50:177–189.
3. Seiler T, Quurke AW. Iatrogenic keratectasia after LASIK in a case of forme fruste keratoconus. *J Cataract Refract Surg*. 1998;24:1007–1009.
4. Binder PS, Lindstrom RL, Stulting RD, et al. Keratoconus and corneal ectasia after LASIK. *J Refract Surg*. 2005;21:749–752.
5. Dawson DG, Randleman JB, Grossniklaus HE, et al. Corneal ectasia after excimer laser keratorefractive surgery: histopathology, ultrastructure, and pathophysiology. *Ophthalmology*. 2008;115:2181–2191e1.

6. Vinciguerra P, Camesasca FI. Prevention of corneal ectasia in laser in situ keratomileusis. *J Refract Surg.* 2001;17(2 suppl):S187–S189.
7. Ambrósio R Jr, Klyce SD, Wilson SE. Corneal topographic and pachymetric screening of keratorefractive patients. *J Refract Surg.* 2003;19:24–29.
8. Oshika T, Klyce SD. Corneal topography in LASIK. *Semin Ophthalmol.* 1998;13: 64–70.
9. Ambrósio R Jr, Wilson SE. Complications of laser in situ keratomileusis: etiology, prevention, and treatment. *J Refract Surg.* 2001;17:350–379.
10. Randleman JB, Woodward M, Lynn MJ, et al. Risk assessment for ectasia after corneal refractive surgery. *Ophthalmology.* 2008;115:37–50.
11. Randleman JB, Trattler WB, Stulting RD. Validation of the ectasia risk score system for preoperative laser in situ keratomileusis screening. *Am J Ophthalmol.* 2008;145:813–818.
12. Chan CC, Hodge C, Sutton G. External analysis of the Randleman ectasia risk factor score system: a review of 36 cases of post LASIK ectasia. *Clin Experiment Ophthalmol.* 2010;38:335–340.
13. Binder PS, Trattler WB. Evaluation of a risk factor scoring system for corneal ectasia after LASIK in eyes with normal topography. *J Refract Surg.* 2010;26:241–250.
14. Duffey RJ, Hardten DR, Lindstrom RL, et al. Ectasia after refractive surgery. *Ophthalmology.* 2008;115:1849. [author reply 49–50].
15. Klein SR, Epstein RJ, Randleman JB, et al. Corneal ectasia after laser in situ keratomileusis in patients without apparent preoperative risk factors. *Cornea.* 2006;25:388–403.
16. Amoils SP, Deist MB, Gous P, et al. Iatrogenic keratectasia after laser in situ keratomileusis for less than −4.0 to −7.0 diopters of myopia. *J Cataract Refract Surg.* 2000;26:967–977.
17. Ambrósio R Jr, Dawson DG, Salomão M, et al. Corneal ectasia after LASIK despite low preoperative risk: tomographic and biomechanical findings in the unoperated, stable, fellow eye. *J Refract Surg.* 2010;26:906–911.
18. Tabbara KF, Kotb AA. Risk factors for corneal ectasia after LASIK. *Ophthalmology.* 2006;113:1618–1622.
19. Belin MW, Ambrósio R Jr. Corneal ectasia risk score: statistical validity and clinical relevance. *J Refract Surg.* 2010;26:238–240.
20. Randleman JB, Russell B, Ward MA, et al. Risk factors and prognosis for corneal ectasia after LASIK. *Ophthalmology.* 2003;110:267–275.
21. Condon PI. 2005 ESCRS Ridley Medal Lecture: will keratectasia be a major complication for LASIK in the long term?. *J Cataract Refract Surg.* 2006;32:2124–2132.
22. Condon PI, O'Keefe M, Binder PS. Long-term results of laser in situ keratomileusis for high myopia: risk for ectasia. *J Cataract Refract Surg* 2007;33:583–590.
23. Geggel HS, Talley AR. Delayed onset keratectasia following laser in situ keratomileusis. *J Cataract Refract Surg.* 1999;25:582–586.
24. Probst LE, Machat JJ. Mathematics of laser in situ keratomileusis for high myopia. *J Cataract Refract Surg.* 1998;24:190–195.
25. Ou RJ, Shaw EL, Glasgow BJ. Keratectasia after laser in situ keratomileusis (LASIK): evaluation of the calculated residual stromal bed thickness. *Am J Ophthalmol.* 2002;134:771–773.
26. Tuli SS, Iyer S. Delayed ectasia following LASIK with no risk factors: is a 300-microm stromal bed enough? *J Refract Surg.* 2007;23:620–622.
27. Binder PS. Analysis of ectasia after laser in situ keratomileusis: risk factors. *J Cataract Refract Surg.* 2007;33:1530–1538.
28. Kim H, Choi JS, Joo CK. Corneal ectasia after PRK: clinicopathologic case report. *Cornea.* 2006;25:845–848.
29. Randleman JB, Stulting RD. Ectasia after photorefractive keratectomy. *Ophthalmology.* 2007;114:396. [author reply 96–97].

30. Mohammadpour M. Corneal ectasia after LASIK in one eye and uneventful PRK in the fellow eye. *J Cataract Refract Surg*. 2007;33:1677. [author reply 77–78].
31. Vinciguerra P, Munoz MI, Camesasca FI, et al. Long-term follow-up of ultrathin corneas after surface retreatment with phototherapeutic keratectomy. *J Cataract Refract Surg*. 2005;31:82–87.
32. Wilson SE, Klyce SD. Advances in the analysis of corneal topography. *Surv Ophthalmol*. 1991;35:269–277.
33. Klyce SD. Corneal topography and the new wave. *Cornea*. 2000;19:723–729.
34. Salomao MQ, Esposito A, Dupps WJ Jr. Advances in anterior segment imaging and analysis. *Curr Opin Ophthalmol*. 2009;20:324–332.
35. Maguire LJ, Bourne WM. Corneal topography of early keratoconus. *Am J Ophthalmol*. 1989;108:107–112.
36. Maeda N, Klyce SD, Tano Y. Detection and classification of mild irregular astigmatism in patients with good visual acuity. *Surv Ophthalmol*. 1998;43:53–58.
37. Wilson SE, Lin DT, Klyce SD, et al. Topographic changes in contact lens-induced corneal warpage. *Ophthalmology*. 1990;97:734–744.
38. Rabinowitz YS, Yang H, Brickman Y, et al. Videokeratography database of normal human corneas. *Br J Ophthalmol*. 1996;80:610–616.
39. Klyce SD. Chasing the suspect: keratoconus. *Br J Ophthalmol*. 2009;93:845–847.
40. Fontes BM, Ambrósio R Jr, Salomao M, et al. Biomechanical and tomographic analysis of unilateral keratoconus. *J Refract Surg*. 2010;26:677–681.
41. Li X, Rabinowitz YS, Rasheed K, et al. Longitudinal study of the normal eyes in unilateral keratoconus patients. *Ophthalmology*. 2004;111:440–446.
42. Saad A, Gatinel D. Topographic and tomographic properties of forme fruste keratoconus corneas. *Invest Ophthalmol Vis Sci*. 2010;51:5546–5555.
43. Saad A, Lteif Y, Azan E, et al. Biomechanical properties of keratoconus suspect eyes. *Invest Ophthalmol Vis Sci*. 2010;51:2912–2916.
44. Amsler M. The "forme fruste" of keratoconus. *Wien Klin Wochenschr*. 1961;73:842–843.
45. Schweitzer C, Roberts CJ, Mahmoud AM, et al. Screening of forme fruste keratoconus with the ocular response analyzer. *Invest Ophthalmol Vis Sci*. 2010;51:2403–2410.
46. Ambrósio R Jr, Dawson DG, Salomao M, et al. Corneal ectasia after LASIK despite low preoperative risk: tomographic and biomechanical findings in the unoperated, stable, fellow eye. *J Refract Surg*. 2010;26:906–911.
47. Ambrósio R Jr, Belin MW. Imaging of the cornea: topography versus tomography. *J Refract Surg*. 2010;26:847–849.
48. Ambrósio R Jr, Tervo T, Wilson SE. LASIK-associated dry eye and neurotrophic epitheliopathy: pathophysiology and strategies for prevention and treatment. *J Refract Surg*. 2008;24:396–407.
49. Smolek MK, Klyce SD, Hovis JK. The Universal Standard Scale: proposed improvements to the American National Standards Institute (ANSI) scale for corneal topography. *Ophthalmology*. 2002;109:361–369.
50. Wilson SE, Klyce SD, Husseini ZM. Standardized color-coded maps for corneal topography. *Ophthalmology*. 1993;100:1723–1727.
51. Rabinowitz YS, McDonnell PJ. Computer-assisted corneal topography in keratoconus. *Refract Corneal Surg*. 1989;5:400–408.
52. Rabinowitz YS, Rasheed K. KISA% index: a quantitative videokeratography algorithm embodying minimal topographic criteria for diagnosing keratoconus. *J Cataract Refract Surg*. 1999;25:1327–1335.
53. Klyce SD, Karon MD, Smolek MK. Screening patients with the corneal navigator. *J Refract Surg*. 2005;21(5 suppl):S617–S622.
54. Maeda N, Klyce SD, Smolek MK, et al. Automated keratoconus screening with corneal topography analysis. *Invest Ophthalmol Vis Sci*. 1994;35:2749–2757.

55. Abad JC, Rubinfeld RS, Del Valle M, et al. Vertical D: a novel topographic pattern in some keratoconus suspects. *Ophthalmology.* 2007;114:1020–1026.
56. Lee BW, Jurkunas UV, Harissi-Dagher M, et al. Ectatic disorders associated with a claw-shaped pattern on corneal topography. *Am J Ophthalmol.* 2007;144: 154–156.
57. Holladay JT. Keratoconus detection using corneal topography. *J Refract Surg.* 2009;25(10 suppl):S958–S962.
58. Li X, Yang H, Rabinowitz YS. Keratoconus: classification scheme based on videokeratography and clinical signs. *J Cataract Refract Surg.* 2009;35:1597–1603.
59. Belin MW, Khachikian SS. An introduction to understanding elevation-based topography: how elevation data are displayed-a review. *Clin Experiment Ophthalmol.* 2009;37:14–29.
60. Khachikian SS, Belin MW. Posterior elevation in keratoconus. *Ophthalmology.* 2009;116:816. [16 e1 author reply 16–17].
61. De Sanctis U, Loiacono C, Richiardi L, et al. Sensitivity and specificity of posterior corneal elevation measured by Pentacam in discriminating keratoconus/subclinical keratoconus. *Ophthalmology.* 2008;115:1534–1539.
62. Ambrósio R Jr. Percentage thickness increase and absolute difference from thinnest to describe thickness profile. *J Refract Surg.* 2010;26:84–86. [author reply 86–87].
63. Ambrósio R Jr, Alonso RS, Luz A, et al. Corneal-thickness spatial profile and corneal-volume distribution: tomographic indices to detect keratoconus. *J Cataract Refract Surg* 2006;32:1851–1859.
64. Luz A, Ursulio M, Castaneda D, et al. Corneal thickness progression from the thinnest point to the limbus: study based on a normal and a keratoconus population to create reference values. *Arq Bras Oftalmol.* 2006;69:579–583.
65. Roberts C. The cornea is not a piece of plastic. *J Refract Surg.* 2000;16:407–413.
66. Luce DA. Determining in vivo biomechanical properties of the cornea with an ocular response analyzer. *J Cataract Refract Surg.* 2005;31:156–162.
67. Roberts C. Biomechanical customization: the next generation of laser refractive surgery. *J Cataract Refract Surg.* 2005;31:2–5.
68. Dupps WJ Jr, Wilson SE. Biomechanics and wound healing in the cornea. *Exp Eye Res.* 2006;83:709–720.
69. Dupps WJ Jr. Biomechanical modeling of corneal ectasia. *J Refract Surg.* 2005;21: 186–190.
70. Dupps WJ Jr. Hysteresis: new mechanospeak for the ophthalmologist. *J Cataract Refract Surg.* 2007;33:1499–1501.
71. Fontes BM, Ambrósio R Jr, Alonso RS, et al. Corneal biomechanical metrics in eyes with refraction of −19.00 to +9.00 D in healthy Brazilian patients. *J Refract Surg.* 2008;24:941–945.
72. Fontes BM, Ambrósio R Jr, Jardim D, et al. Corneal biomechanical metrics and anterior segment parameters in mild keratoconus. *Ophthalmology.* 2010;117: 673–679.
73. Shah S, Laiquzzaman M, Bhojwani R, et al. Assessment of the biomechanical properties of the cornea with the ocular response analyzer in normal and keratoconic eyes. *Invest Ophthalmol Vis Sci.* 2007;48:3026–3031.
74. Pepose JS, Feigenbaum SK, Qazi MA, et al. Changes in corneal biomechanics and intraocular pressure following LASIK using static, dynamic, and noncontact tonometry. *Am J Ophthalmol.* 2007;143:39–47.
75. Ortiz D, Pinero D, Shabayek MH, et al. Corneal biomechanical properties in normal, post-laser in situ keratomileusis, and keratoconic eyes. *J Cataract Refract Surg.* 2007;33:1371–1375.

76. Shah S, Laiquzzaman M, Yeung I, et al. The use of the ocular response analyser to determine corneal hysteresis in eyes before and after excimer laser refractive surgery. *Cont Lens Anterior Eye*. 2009;32:123–128.
77. Shah S, Laiquzzaman M. Comparison of corneal biomechanics in pre and post-refractive surgery and keratoconic eyes by ocular response analyser. *Cont Lens Anterior Eye*. 2009;32:129–132. [quiz 51].
78. Elsheikh A, Wang D, Pye D. Determination of the modulus of elasticity of the human cornea. *J Refract Surg*. 2007;23:808–818.
79. Kerautret J, Colin J, Touboul D, et al. Biomechanical characteristics of the ectatic cornea. *J Cataract Refract Surg*. 2008;34:510–513.
80. Reinstein DZ, Archer TJ, Gobbe M. Stability of LASIK in topographically suspect keratoconus confirmed non-keratoconic by Artemis VHF digital ultrasound epithelial thickness mapping: 1-year follow-up. *J Refract Surg*. 2009;25:569–577.